JOURNAL OF RENEWABLE ENERGY AND SMART GRID TECHNOLOGY

Vol. 20, No. 2, July-December 2025

Modeling and Analysis of Energy Micro-Grids Using Hybrid Petri Nets

Khouloud Soltani[1,2*], Hajer Mlayeh[1], Atef Khedher[1]

[1]Laboratory of Advanced Technology and Intelligent Systems, University of Sousse, Sousse 4023, Tunisia
[2]National Engineering School of Gabes, University of Gabes, Gabes 6072, Tunisia

***Corresponding author's email**: soltani_khouloud@yahoo.com

Article info:

Received: 17 May 2025
Revised: 6 July 2025
Accepted: 13 August 2025
DOI:
10.69650/rast.2025.262183

Keywords:

Microgrids Systems
Hybrid Petri Nets
Linear Algebraic Model
Dater Approach
Counter Approach
Hybrid Dynamic

ABSTRACT

Hybrid Petri nets (HPN) are frequently used to model and study hybrid systems, i.e. those with both discrete (events, state changes) and continuous (flows, changing physical variables) dynamics. In recent years, their field of application has been extended to energy systems, and in particular to the modeling of electrical microgrids. These microgrids are often powered by renewable energy sources, whose operation is variable and subject to environmental constraints. With this in mind, the present study suggests an HPN-based modeling technique to illustrate the operation of an electrical microgrid that integrates a photovoltaic installation associated with a battery storage system. The idea is to capture the complex interaction between various energy sources, storage units, energy demand and possible complementary sources. The associated mathematical model is based on a linear algebraic representation of type $Ax \leq b$, which formalizes the system's constraints, tracks the evolution of its state over time, and anticipates its future behavior. Simultaneously, a state observer is developed with the intention of evaluating the current Petri net marking exclusively from observable results, in order to deduce an accurate estimate of the internal state. By comparing the simulation results with the estimation results, we are able to assess the robustness and accuracy of the suggested model. This research is part of an approach aimed at optimizing and intelligently supervising sustainable energy systems.

1. Introduction

With the gradual depletion of fossil fuels and increasing pollution, the need for sustainable, accessible energy systems is becoming ever more pressing worldwide. the development of green energies, such as solar, wind, hydroelectric and geothermal power, is crucial to the energy transition, as it reduces our reliance on fossil fuels. With this in mind, microgrids are a sensible way of incorporating these renewable energies (RES) into electricity grids, thereby guaranteeing a stable, high-level supply [1-6].

A microgrid is an autonomous energy production system consisting of distributed generators, storage devices and consumers, connected to the main grid via a common coupling point (CCP). It is capable of operating in grid-connected or stand-alone mode, guaranteeing a constant energy supply even during disturbances on the main grid. What's more, the modeling and examination of these systems represent a crucial challenge due to their hybrid nature, combining continuous dynamics such as energy flows with discrete incidents such as outages, failures or state changes [7-9].

Energy microgrids are, by nature, hybrid systems, comprising both continuous elements (such as energy flows, voltages or currents) and discrete elements (such as switching operations, control decisions or logic events). The temporal evolution of such a system depends directly on the interaction between all its components.

In this context, hybrid Petri nets (HPN) are a particularly well-suited formalism for modeling such systems. Indeed, they enable continuous dynamics and discrete events to be represented simultaneously within the same structure. This capability is essential to accurately capture the overall behavior of a microgrid, particularly when coordinating energy sources, managing storage, or implementing complex control strategies. HPN modeling thus enables improved simulation, state estimation and anomaly detection in distributed energy systems.

Conventional power system modeling methods, such as matrix state analysis, allow the continuous dynamics of energy networks to be represented. However, they often tend to ignore punctual events that could affect these dynamics, such as changes in the position of transformer taps or the regulation of battery charge/discharge cycles. A more appropriate option would be to use HPN, which are able to represent discrete and continuous aspects of energy systems in an integrated way [10-12]. Section 3 will provide a more in-depth description of this method. By integrating discrete and continuous elements within a single structure, HPNs offer the possibility of faithfully representing energy flows, operational decisions and state transitions in microgrids. This approach simplifies the study of the complicated interactions between solar power generation and storage management, while optimizing the system as a whole [13-17].

As part of this research, a modeling approach is suggested, based on an algebraic linear model of the type $Ax \leq b$, with the aim of illustrating microgrid dynamics. A state estimator is also developed to judge the accuracy of predictions, by confronting simulation results with data from estimation [18-21]. The effectiveness of this technique is demonstrated by a case study, attesting to its relevance for the analysis and optimization of energy flows.

This research concerns the implementation of state and input estimators derived from counter and dater methods, aimed at enhancing the monitoring and management skills of hybrid systems. These techniques take advantage of the inherent structure of HPN to faithfully represent the progression of system states and input transitions, even in the case of incomplete or dubious observations.

The counter approach is specially designed for discrete-event systems such as microgrids, where tracking events such as switching, activation or resource management is essential. The dater approach, on the other hand, emphasizes the temporal accuracy of events and transitions, enabling detailed reconstruction of system trajectories through time.

This research presents a hybrid modeling and evaluation framework for energy microgrids, based on HPN. By combining counter- and dating approaches for state and input evaluation, our approach offers a mathematically sound and practically applicable tool for monitoring, analyzing and managing microgrid systems under observable and uncertain conditions. Its uniqueness derives from the incorporation of the HPN structure into the algebraic inequalities, enabling robust simulation and real-time estimation capability, illustrated by a concrete example of a 4-DG microgrid. It is particularly significant to opt for a microgrid with four distributed generators (4-DG) as the case study subject. It represents the true complexity of modern decentralized energy systems, where several diverse energy sources (such as solar, wind, battery storage and diesel backup) are required to operate simultaneously and in a coordinated fashion. To model such a configuration correctly, it is necessary to take into account asynchronous behavior, changing production rates and evolving demand profiles, all of which are inherently hybrid. By implementing our estimation framework in this multi-source environment, we demonstrate the robustness and scalability of our approach. Not only does this case study confirm the theoretical model, it also establishes our method as an effective resource for use in intelligent energy management systems (EMS), under both normal and disturbed operating conditions.

By presenting the estimation problem in the form of linear matrix inequalities (LMI), the suggested estimators simultaneously guarantee the robustness and stability of the estimation process. This combined method proves to be an effective tool for real-time monitoring, error identification and efficiency assessment of complex energy systems.

The article begins with an introduction, followed by a literature review detailed in section 2. Section 3 focuses on the introduction of HPN and the notations employed. The core of section 4 is the suggested state model, while the design of the state observer is detailed in section 5. In the sixth section, the model and observer are implemented on a microgrid in the context of a simulation. Section 7 concludes with a comparative analysis of the results.

2. Related literature

Much research has been devoted to the modeling and analysis of microgrids using HPN, to improve energy management and accurately reflect the complex dynamics inherent in these systems, this research exploits the ability of Hybrid Petri Networks (HPN) to represent both discrete events and continuous evolutions, two fundamental aspects of microgrids.

The research highlighted in [22] demonstrates this approach by suggesting an HPN-based technique for energy management of an autonomous microgrid, whose main aim is to improve energy distribution according to user requirements.

Indeed, they propose to use HPN model of a micro grid to take an hourly decision about dispatching energy between the connected installation according to the need of each installation. Also, in [23], an HPN based approach is used to model an intelligent microgrid based on a principle of power balance within a bus, enabling modular integration of energy sources and storage. Finally, [24] focuses on the variability of renewable sources, generating a system state evolution diagram from the HPN model to better analyze uncertainties. The authors in [12] used the reachability graph of the proposed HPN to synchronize between four energy sources.

However, unlike these approaches, our work proposes a rigorous formulation based on a linear algebraic model $Ax \leq b$ to represent the hybrid dynamics of the system. In addition, we develop a state observer enabling not only accurate estimation of system evolution, but also input vector reconstruction and anomaly detection. This dual modeling (simulation and estimation) is not covered in [22-24]. Indeed, the work presented in [22-24] analyze the system behavior according to the evolution of the HPN marking, but in our work, we consider the number of firings of each transition at each time as the system state if the counter approach is considered. Only the initial marking is supposed known.

Our results stand out for their high accuracy, and better analytical significance, in line with the formal structure of the proposed model. Comparison between simulated and estimated results shows rapid convergence of residuals, illustrating the robustness and high performance of our method compared with existing work.

In addition to the above-mentioned contributions, a large body of research has investigated HPN-based structures for supervisory control and fault resilience in decentralized energy systems. For example, [25] investigates a hierarchical control structure combining PN with rule-based logic to coordinate multiple energy sources in a smart microgrid. Although this method is effective for modular control, it suffers from the absence of a quantitative evaluation framework and does not take into account state reconstruction in situations of partial observability. Thus, [26] suggests an HPN model for power quality control, focusing on event-based behavior, but without addressing the analytical interplay between discrete and continuous domains necessary for dynamic estimation.

Furthermore, [27] employed HPN to model energy exchanges between subsystems, focusing on graphical representation and scenario testing. However, this research remains essentially descriptive and lacks formal evaluation tools or mathematical verification of system operation. Our method, however, combines behavioral simulation and analytical estimation in a unified context, enabling further analysis of microgrid performance under a variety of input conditions and structural configurations.

3. HPN formalism

A HPN is a method for representing and analyzing dynamic systems, integrating both discrete aspects (such as events and state changes) and continuous aspects (such as the evolution of physical variables over time). It is an extension of traditional Petri nets, developed to integrate continuous elements frequently encountered in physical, industrial or energy systems. In a PHN:

- Places can accommodate either discrete markings (integers, symbolizing a certain number of tokens), or continuous markings (real values, which can represent degrees of energy or fluids, for example).
- Transitions can be discrete (triggered by events) or continuous (operating with speeds or flows).
- The arcs linking locations and transitions are assigned weights, which define the firing conditions and dynamics of token transfer.

Differential or constant-velocity equations are frequently used to represent continuous dynamics, enabling us to simulate the temporal progression of various flows (production, energy, temperature, etc.).

This type of network is particularly suitable for modeling complex hybrid systems such as electrical microgrids, industrial automation processes, transportation systems or biological systems. It offers an integrated approach to capturing the interaction between (discrete) control logic and (continuous) physical phenomena, while providing tools for structured analysis, simulation, verification and observation.

According to [28], a HPN is defined as a structure comprising the following elements:

$$N = (P, T, P^{re}, P^{ost}, C, D)$$

with:

- The set of places *P* encompasses two subcategories: discrete places P_d and continuous places P_c, whose cardinalities are respectively noted as n_d and n_c
- The set of locations amounts to n. Each location is designated by the label P_i with $i \in \{1, ..., n\}$ [29-32]. In the graphical context, discrete locations are symbolized by single circles, while continuous locations are depicted by two concentric circles.
- *T* transitions are also classified into two types: discrete T_d, transitions and continuous T_c transitions. Segments illustrate discrete transitions, while double contoured rectangles depict continuous transitions.
- The weights assigned to the arcs in the network are defined by the pre and post incidence functions. The first of these functions is specifically designed for continuous squares, while the second applies to discrete squares.

$$P_c \times T \to R^+, \quad P_d \times T \to N$$

In a HPN, the simultaneous presence of discrete and continuous dynamics allows four kinds of interaction between places and transitions. A discrete location can be associated with either a discrete or a continuous transition. It is also possible to link a continuous place to either a discrete transition or a continuous transition. These various configurations offer the possibility of accurately representing the complex interactions specific to hybrid systems.

A HPN is considered to be well structured if, for $t \in t_c$ and $p \in p_d$, the pre-incidence and post-incidence functions satisfy the following condition:

$$P^{re}(p,t) = P^{ost}(p,t)$$

This condition ensures that the activation of a continuous transition does not affect the marking of discrete places [33-34].

The HPN incidence matrix can therefore be defined as follows:

$$w(p,t) = P^{ost}(p,t) - P^{re}(p,t) \quad (1)$$

$$w = w\_\{P^{ost}\} - w\_\{P^{re}\} \quad (2)$$

We use the notation x to symbolize internal transitions, u for input transitions and y for output transitions, in order to differentiate them.

We also denote T_i as the duration related to location P_i, which corresponds to the time a tag remains in that location.

4. State model design

4.1. Objective

The aim of this section is to develop a new state model for analyzing the temporal evolution of the microgrids state and outputs. The hybrid system requires a model that can simultaneously represent discrete event-related behavior (such as mode changes and control actions) as well as continuous evolution (such as energy accumulation or power flow). To remedy this, we propose a formal model structure producing two key linear inequalities: the first enables us to estimate the internal state of the system, and the second provides a mechanism for calculating system outputs based on transition triggers and model structure. These inequalities form the basis of our estimation strategy.

The model established is analogous to a continuous state-space representation, but adapted to the hybrid structure of the HPN. The state vector is not based on markings as in classical Petri net analysis, but on the cumulative number of transition triggers, offering greater flexibility and abstraction in systems with limited observability. The model is developed using a complementary method: the counter approach, which focuses on quantifying events.

4.2. Counter approach

The counter-based approach is a modeling technique that focuses on counting the occurrences of each transition in a hybrid Petri net over time. Rather than tracking the instantaneous marking of locations, this method relies on the accumulation of transition triggers, reflecting the cumulative behavior of the system and providing a useful abstraction for hybrid systems such as microgrids.

In this approach, the state of the system is represented by a vector *x(t),* where each component corresponds to the total number of triggers of a specific transition up to time *t.* This makes it possible to track the evolution of the system. This makes it possible to track the evolution of the system as events (such as energy production, storage charging or load switching) occur repeatedly. The advantage is a continuous, monotonic view of system activity, perfect for estimation and analysis.

State evolution is then governed by a set of linear inequalities, usually expressed as:

$$Ax(t) \leq b(t)$$

Here, *An* incorporates the system's structural and operational constraints, such as energy balances, priority rules or capacity constraints. The vector *b(t)* includes time-varying bounds or thresholds, possibly derived from system specifications or real-time measurements.

This formulation makes it possible to capture system behavior even when certain variables (such as markings or exact energy levels) are not directly observable. It is particularly effective in detection-limited scenarios, where only events such as "generator on" or "battery charging" are available.

In the context of a microgrid, transitions can model discrete decisions such as connecting a generator, triggering a battery discharge or redirecting energy to a critical load. By accounting for these actions over time, the counter-based approach enables energy consumption trends to be estimated, anomalies to be detected and energy allocation to be optimized.

What's more, this modeling framework integrates perfectly with estimation algorithms, enabling the reconstruction of internal dynamics and input behaviors from observed events. The counter representation thus serves as the basis for the observer design presented later in this article.

The matrices $w_{xx}^{+}, w_{xy}^{+}, w_{vx}^{+}, w_{vx}^{-}, w_{xx}^{-}, w_{xy}^{-}, w_{vy}^{+}$ and w_{vy}^{-} which symbolize components of the global incidence matrix w, are determined by the equations below:

$$w_{vx}^{+} = \begin{pmatrix} w_{vx}^{+cc} & w_{vx}^{+cd} \\ w_{vx}^{+dc} & w_{vx}^{+dd} \end{pmatrix}, w_{vx}^{-} = \begin{pmatrix} w_{vx}^{-cc} & w_{vx}^{-cd} \\ w_{vx}^{-dc} & w_{vx}^{-dd} \end{pmatrix} \quad (3a)$$

$$w_{xx}^{+} = \begin{pmatrix} w_{xx}^{+cc} & w_{xx}^{+cd} \\ w_{xx}^{+dc} & w_{xx}^{+dd} \end{pmatrix}, w_{xx}^{-} = \begin{pmatrix} w_{xx}^{-cc} & w_{xx}^{-cd} \\ w_{xx}^{-dc} & w_{xx}^{-dd} \end{pmatrix} \quad (3b)$$

$$w_{xy}^{+} = \begin{pmatrix} w_{xy}^{+cc} & w_{xy}^{+cd} \\ w_{xy}^{+dc} & w_{xy}^{+dd} \end{pmatrix}, w_{xy}^{-} = \begin{pmatrix} w_{xy}^{-cc} & w_{xy}^{-cd} \\ w_{xy}^{-dc} & w_{xy}^{-dd} \end{pmatrix} \quad (3c)$$

$$w_{vy}^{+} = \begin{pmatrix} w_{vy}^{+cc} & w_{vy}^{+cd} \\ w_{vy}^{+dc} & w_{vy}^{+dd} \end{pmatrix}, w_{vy}^{-} = \begin{pmatrix} w_{vy}^{-cc} & w_{vy}^{-cd} \\ w_{vy}^{-dc} & w_{vy}^{-dd} \end{pmatrix} \quad (3d)$$

where the index cc refers to continuous transitions and index cd refers to discrete transitions. In addition index cc models the link between continuous places, index dd models the link between discrete places, index dc describes the link from discrete to continuous places and cd models the link from continuous to discrete places.

In a Petri net, the set of places can be divided into four distinct subgroups, each representing a specific type of connection between transitions. The set P_{vx} gathers the places that lie between input transitions and internal transitions. The subset P_{xx} encompasses the places that lie between two internal transitions. Subsequently, the locations between internal and output transitions are combined in the group P_{xy}. Finally, transitions that establish a direct connection between inputs and outputs are embedded in P_{vy}. Based on these notations, we can then establish the following inequalities:

$$\begin{pmatrix} -w_{vx}^{+} & -w_{vx}^{-} \end{pmatrix} \begin{pmatrix} v(t) \\ x(t) \end{pmatrix} \leq \begin{pmatrix} m_{vx} \\ m_{vx} \end{pmatrix} \quad (4)$$

$$\begin{pmatrix} -w_{xx}^{+} & -w_{xx}^{-} \end{pmatrix} \begin{pmatrix} x(t-1) \\ x(t) \end{pmatrix} \leq \begin{pmatrix} m_{xx} \\ m_{xx} \end{pmatrix} \quad (5)$$

$$\begin{pmatrix} -w_{xy}^{+} & -w_{xy}^{-} \end{pmatrix} \begin{pmatrix} x(t) \\ y(t) \end{pmatrix} \leq \begin{pmatrix} m_{xy} \\ m_{xy} \end{pmatrix} \quad (6)$$

$$\begin{pmatrix} -w_{vy}^{+} & -w_{vy}^{-} \end{pmatrix} \begin{pmatrix} v(t) \\ y(t) \end{pmatrix} \leq \begin{pmatrix} m_{vy} \\ m_{vy} \end{pmatrix} \quad (7)$$

Inequality (4) describes the interactions between input transitions and internal transitions, while inequality (5) illustrates the dependencies among internal transitions. Inequality (6) illustrates the relationships between internal transitions and end transitions. In situations where loci establish a direct link between input and output transitions, they are defined by inequality (7).

Remark 1: Inequalities (4) to (7) can be elaborated and specified, resulting in a series of extended inequalities identified from (8) to (15).

$$\begin{aligned} &-w_{vx}^{+cc} v_c(t) - w_{vx}^{+cd} v_d(t) + w_{vx}^{-cc} x_c(t) \\ &+ w_{vx}^{-cd} x_d(t) \leq (m_{vx}) \end{aligned} \quad (8)$$

$$\begin{aligned} &-w_{ux}^{+dc} v_c(t) - w_{ux}^{+dd} v_d(t) + w_{ux}^{-dc} x_c(t) \\ &+ w_{ux}^{-dd} x_d(t) \leq (m_{vx}) \end{aligned} \quad (9)$$

$$\begin{aligned} &-w_{xx}^{+cc} x_c(t-1) - w_{xx}^{+cd} x_d(t-1) + w_{xx}^{-cc} x_c(t) \\ &+ w_{xx}^{-cd} x_d(t) \leq (m_{xx}) \end{aligned} \quad (10)$$

$$\begin{aligned} &-w_{xx}^{+dc} x_c(t-1) - w_{xx}^{+dd} x_d(t-1) \\ &\qquad + w_{xx}^{-dc} x_c(t) \\ &+ w_{xx}^{-dd} x_d(t) \leq (m_{xx}) \end{aligned} \quad (11)$$

$$\begin{aligned} &-w_{xy}^{+cc} x_c(t) - w_{xy}^{+cd} x_d(t) + w_{xy}^{-cc} y_c(t) \\ &+ w_{xy}^{-cd} y_d(t) \leq (m_{xy}) \end{aligned} \quad (12)$$

$$\begin{aligned} &-w_{xy}^{+dc} x_c(t) - w_{xy}^{+dd} x_d(t) + w_{xy}^{-dc} x_c(t) \\ &+ w_{xy}^{-dd} x_d(t) \leq (m_{xy}) \end{aligned} \quad (13)$$

$$\begin{aligned} &-w_{vy}^{+cc} v_c(t) - w_{vy}^{+cd} v_d(t) + w_{vy}^{-cc} y_c(t) \\ &+ w_{vy}^{-cd} y_d(t) \leq (m_{vy}) \end{aligned} \quad (14)$$

$$\begin{aligned} &-w_{vy}^{+dc} v_c(t) - w_{vy}^{+dd} v_d(t) + w_{vy}^{-dc} y_c(t) \\ &+ w_{vy}^{-dd} y_d(t) \leq (m_{vy}) \end{aligned} \quad (15)$$

The system must have an ascending time progression, or at least not be in decline. To guarantee this property, inequalities (16) to (19) are implemented.

$$x_c(t-1) \leqslant x_c(t) \Rightarrow -x_c(t) \leq -x_c(t-1) \quad (16)$$

$$x_d(t-1) \leqslant x_d(t) \Rightarrow -x_d(t) \leq -x_d(t-1) \quad (17)$$

$$v_c(t) \leqslant y_c(t) \Rightarrow -y_c(t) \leq -v_c(t) \quad (18)$$

$$v_d(t) \leqslant y_d(t) \Rightarrow -y_d(t) \leq -v_d(t) \quad (19)$$

Inequalities (8) to (19) are gathered to obtain inequalities (20) and (21).

The inequality (20) provides an upper bound for the state vector *x(t),* which represents the simulated time evolution of the system's internal state. On the other hand, inequality (21) gives an upper bound for the output *y(t),* which represents the simulated trajectory of the system over time.

$$\begin{aligned} &\begin{pmatrix} w_{vx}^{-cc} & w_{vx}^{-cc} \\ w_{vx}^{-dc} & w_{vx}^{-dd} \\ w_{xx}^{-cc} & w_{xx}^{-cd} \\ w_{xx}^{-dc} & w_{xx}^{-dd} \\ -I & -I \end{pmatrix} \begin{pmatrix} x_c(t) \\ x_d(t) \end{pmatrix} \leq \begin{pmatrix} m_{vx} \\ m_{vx} \\ m_{xx} \\ m_{xx} \\ 0 \end{pmatrix} + \\ &\begin{pmatrix} w_{vx}^{+cc} & w_{vx}^{+cd} & 0 & 0 \\ w_{vx}^{+dc} & w_{vx}^{+dd} & 0 & 0 \\ 0 & 0 & w_{xx}^{+cc} & w_{xx}^{+cd} \\ 0 & 0 & w_{xx}^{+dc} & w_{xx}^{+dd} \\ 0 & 0 & -I & -I \end{pmatrix} \begin{pmatrix} v_c(t) \\ v_d(t) \\ x_c(t-1) \\ x_d(t-1) \end{pmatrix} \end{aligned} \quad (20)$$

$$\begin{pmatrix} w_{xy}^{-cc} & w_{xy}^{-cd} \\ w_{xy}^{-dc} & w_{xy}^{-dd} \\ w_{vy}^{-cc} & w_{vy}^{-cd} \\ w_{vy}^{-dc} & w_{vy}^{-dd} \\ -I & -I \end{pmatrix} \begin{pmatrix} y_c(t) \\ y_d(t) \end{pmatrix} \leq \begin{pmatrix} m_{xy} \\ m_{xy} \\ m_{vy} \\ m_{vy} \\ 0 \end{pmatrix} + \begin{pmatrix} w_{xy}^{+cc} & w_{xy}^{+cd} & 0 & 0 \\ w_{xy}^{+dc} & w_{xy}^{+dd} & 0 & 0 \\ 0 & 0 & w_{vy}^{+cc} & w_{vy}^{+cd} \\ 0 & 0 & w_{vy}^{+dc} & w_{vy}^{+dd} \\ 0 & 0 & -I & -I \end{pmatrix} \begin{pmatrix} x_c(t) \\ x_d(t) \\ v_c(t) \\ v_d(t) \end{pmatrix} \quad (21)$$

With regard to inequalities (20) and (21), we can therefore suggest the following state model:

$$\begin{cases} [A_1^c A_1^d] \begin{bmatrix} x_c(t) \\ x_d(t) \end{bmatrix}, , [A_2^c A_2^d] \begin{bmatrix} x_c(t-1) \\ x_d(t-1) \end{bmatrix} + [B_1^c B_1^d] \begin{bmatrix} v_c(t) \\ v_d(t) \end{bmatrix} + [M_x] \\ [C_1^c C_1^d] \begin{bmatrix} y_c(t) \\ y_d(t) \end{bmatrix}, , [C_2^c C_2^d] \begin{bmatrix} x_c(t) \\ x_d(t) \end{bmatrix} + [D_1^c D_1^d] \begin{bmatrix} v_c(t) \\ v_d(t) \end{bmatrix} + [M_y] \end{cases} \quad (22)$$

With:

$$A_1^c = \begin{pmatrix} w_{vx}^{-cc} \\ w_{vx}^{-dc} \\ w_{xx}^{-cc} \\ w_{xx}^{-dc} \\ -I \end{pmatrix}, A_2^c = \begin{pmatrix} 0 \\ 0 \\ -w_{xx}^{+cc} \\ -w_{xx}^{+dc} \\ -I \end{pmatrix}, M_x = \begin{pmatrix} m_{vx} \\ m_{vx} \\ m_{xx} \\ m_{xx} \\ 0 \end{pmatrix},$$
$$B_1^c = \begin{pmatrix} -w_{vx}^{+cc} \\ -w_{vx}^{+dc} \\ 0 \\ 0 \\ 0 \end{pmatrix} \quad (23)$$

$$A_1^d = \begin{pmatrix} w_{vx}^{-cd} \\ w_{vx}^{-dd} \\ w_{xx}^{-cd} \\ w_{xx}^{-dd} \\ -I \end{pmatrix}; A_2^d = \begin{pmatrix} 0 \\ 0 \\ -w_{xx}^{+cd} \\ -w_{xx}^{+dd} \\ -I \end{pmatrix}, \; B_2^d = \begin{pmatrix} -w_{vx}^{+cd} \\ -w_{vx}^{+dd} \\ 0 \\ 0 \\ 0 \end{pmatrix} \quad (24)$$

$$C_1^c = \begin{pmatrix} w_{xy}^{-cc} \\ w_{xy}^{-dc} \\ w_{vy}^{-cc} \\ w_{vy}^{-dc} \\ -I \end{pmatrix}; C_2^c = \begin{pmatrix} -w_{xy}^{+cc} \\ -w_{xy}^{+dc} \\ 0 \\ 0 \\ -I \end{pmatrix}; M_y = \begin{pmatrix} m_{xy} \\ m_{xy} \\ m_{vy} \\ m_{vy} \\ 0 \end{pmatrix};$$
$$D_1^c = \begin{pmatrix} 0 \\ 0 \\ -w_{vx}^{+cc} \\ -w_{vx}^{+dc} \\ 0 \end{pmatrix} \quad (25)$$

$$C_1^d = \begin{pmatrix} w_{xy}^{-cd} \\ w_{xy}^{-dd} \\ w_{vy}^{-cd} \\ w_{vy}^{-dd} \\ -I \end{pmatrix}; C_2^d = \begin{pmatrix} -w_{xy}^{+cd} \\ -w_{xy}^{+dd} \\ 0 \\ 0 \\ -I \end{pmatrix}, \; D_1^d = \begin{pmatrix} 0 \\ 0 \\ -w_{vx}^{+cd} \\ -w_{vx}^{+dd} \\ 0 \end{pmatrix} \quad (26)$$

The trajectory and dynamic behavior of the system may be analyzed by the simulation of the state model represented by equation (22). It makes it possible to calculate the number of transition firings $x_c(t)$, $x_d(t)$, $y_c(t)$, $y_d(t)$ based on the system inputs $v_c(t)$, $x_d(t)$ and the prior firings x_c(t-1), $x_d(t-1)$, $y_c(t-1)$ and $y_d(t-1)$. The system's status at a specific time *t* is characterized by the number of firings.

- *x(t):* System state indicating the accumulated total of internal transition triggers at time *t.*
- *v(t):* Input vector indicating the number of triggers of input transitions at time *t*.
- *y(t):* Output vector indicating the number of output transition triggers at time *t.*
- *A, B, C:* Incidence submatrices from the HPN structure.
- *b(t):* Vector representing restrictions or constraints at time *t,* based on system specifications.

3.4. Dater approach

The dating approach is based on the use of time stamps (dates) linked to transition events, thus facilitating a temporal reconstruction of the system's operating sequences. In a hybrid Petri net system, the dynamics are both continuous and discrete. The dater method takes advantage of this duality by exploiting the time intervals associated with transitions to constrain and estimate the evolution of network marking over time.

The date-based approach assumes that each transition is linked to a potential start date. The state vector indicates these potential start dates. System events are modeled using timed transitions that trigger an action on a specific date or when certain conditions are met.

Using the matrices established in (3) and the symbols presented earlier, we can state the following inequalities:

$$(w_{vx}^{+} \quad -w_{vx}^{-}) \begin{pmatrix} v(t) \\ x(t) \end{pmatrix} \leq \begin{pmatrix} -T_{vx} \\ -T_{vx} \end{pmatrix} \quad (27)$$

$$(w_{xx}^{+} \quad -w_{xx}^{-}) \begin{pmatrix} x(t-1) \\ x(t) \end{pmatrix} \leq \begin{pmatrix} -T_{xx} \\ -T_{xx} \end{pmatrix} \quad (28)$$

$$(w_{xy}^{+} \quad -w_{xy}^{-}) \begin{pmatrix} x(t) \\ y(t) \end{pmatrix} \leq \begin{pmatrix} -T_{xy} \\ -T_{xy} \end{pmatrix} \quad (29)$$

$$(w_{vy}^{+} \quad -w_{vy}^{-}) \begin{pmatrix} v(t) \\ y(t) \end{pmatrix} \leq \begin{pmatrix} -T_{vy} \\ -T_{vy} \end{pmatrix} \quad (30)$$

The input transition and internal transitions are linked by inequality (27). Inequality (28) highlights the interactions between internal transitions, while inequality (29) illustrates the links between internal transitions and outputs. In the case where a hybrid Petri net has places that link input and output transitions, these connections are represented by inequality (30).

Remark 3: We can also extend inequalities (27) to (30), which gives rise to the following extended inequalities:

$$w_{vx}^{+cc} v_c(k) + w_{vx}^{+cd} v_d(k) - w_{vx}^{-cc} x_c(k) - w_{vx}^{-cd} x_d(k) \leq (-T_{vx}) \quad (31)$$

$$w_{vx}^{+dc} v_c(k) + w_{ux}^{+dd} v_d(k) - w_{ux}^{-dc} x_c(k) - w_{ux}^{-dd} x_d(k) \leq (-T_{vx}) \quad (32)$$

$$w_{xx}^{+cc} x_c(k-1) + w_{xx}^{+cd} x_d(k-1) - w_{xx}^{-cc} x_c(k) - w_{xx}^{-cd} x_d(k) \leq (-T_{xx}) \quad (33)$$

$$w_{xx}^{+dc} x_c(k-1) + w_{xx}^{+dd} x_d(k-1) - w_{xx}^{-dc} x_c(k) - w_{xx}^{-dd} x_d(k) \leq (-T_{xx}) \quad (34)$$

$$w_{xy}^{+cc} x_c(k) + w_{xy}^{+cd} x_d(k) - w_{xy}^{-cc} y_c(k) - w_{xy}^{-cd} y_d(k) \leq (-T_{xy}) \quad (35)$$

$$w_{xy}^{+dc} x_c(k) + w_{xy}^{+dd} x_d(k) - w_{xy}^{-dc} x_c(k) - w_{xy}^{-dd} x_d(k) \leq (-T_{xy}) \quad (36)$$

$$w_{vy}^{+cc} v_c(k) + w_{vy}^{+cd} v_d(k) - w_{vy}^{-cc} y_c(k) - w_{uy}^{-cd} y_d(k) \leq (-T_{vy}) \quad (37)$$

$$w_{vy}^{+dc} v_c(k) + w_{vy}^{+dd} v_d(k) - w_{vy}^{-dc} y_c(k) - w_{vy}^{-dd} y_d(k) \leq (-T_{vy}) \quad (38)$$

System direction must be non-decreasing over time. To guarantee this behavior, the following disparities are integrated.

$$x_c(k-1) \leqslant x_c(k) \Rightarrow -x_c(k) \leq -x_c(k-1) \quad (39)$$

$$x_d(k-1) \leqslant x_d(k) \Rightarrow -x_d(k) \leq -x_d(k-1) \quad (40)$$

$$v_c(k) \leqslant y_c(k) \Rightarrow -y_c(k) \leq -v_c(k) \quad (41)$$

$$v_d(k) \leqslant y_d(k) \Rightarrow -y_d(k) \leq -v_d(k) \quad (42)$$

In order to represent the discrete and continuous state of the system as well as its output, constraints (39) to (42) are consolidated into constraints (43) and (44).

$$\begin{pmatrix} -w_{vx}^{-cc} & -w_{vx}^{-cc} \\ -w_{vx}^{-dc} & -w_{vx}^{-dd} \\ -w_{xx}^{-cc} & -w_{xx}^{-cd} \\ -w_{xx}^{-dc} & -w_{xx}^{-dd} \\ -I & -I \end{pmatrix} \begin{pmatrix} x_c(k) \\ x_d(k) \end{pmatrix} \leq \begin{pmatrix} -T_{vx} \\ -T_{vx} \\ -T_{xx} \\ -T_{xx} \\ 0 \end{pmatrix} - \begin{pmatrix} w_{vx}^{+cc} & w_{vx}^{+cd} & 0 & 0 \\ w_{vx}^{+dc} & w_{vx}^{+dd} & 0 & 0 \\ 0 & 0 & w_{xx}^{+cc} & w_{xx}^{+cd} \\ 0 & 0 & w_{xx}^{+dc} & w_{xx}^{+dd} \\ 0 & 0 & -I & -I \end{pmatrix} \begin{pmatrix} v_c(k) \\ v_d(k) \\ x_c(k-1) \\ x_d(k-1) \end{pmatrix} \quad (43)$$

$$\begin{pmatrix} -w_{xy}^{-cc} & -w_{xy}^{-cc} \\ -w_{xy}^{-dc} & -w_{xy}^{-dd} \\ -w_{vy}^{-cc} & -w_{vy}^{-cd} \\ -w_{vy}^{-dc} & -w_{vy}^{-dd} \\ -I & -I \end{pmatrix} \begin{pmatrix} y_c(k) \\ y_d(k) \end{pmatrix} \leq \begin{pmatrix} -T_{xy} \\ -T_{xy} \\ -T_{vy} \\ -T_{vy} \\ 0 \end{pmatrix} - \begin{pmatrix} w_{xy}^{+cc} & w_{xy}^{+cd} & 0 & 0 \\ w_{xy}^{+dc} & w_{xy}^{+dd} & 0 & 0 \\ 0 & 0 & w_{vy}^{+cc} & w_{vy}^{+cd} \\ 0 & 0 & w_{vy}^{+dc} & w_{vy}^{+dd} \\ 0 & 0 & -I & -I \end{pmatrix} \begin{pmatrix} x_c(k) \\ x_d(k) \\ v_c(k) \\ v_d(k) \end{pmatrix} \quad (44)$$

Inequality (43) provides an upper bound estimate for the state vector *x(k),* illustrating the temporal progression of the system's internal state. At the same time, inequality (44) serves as an upper bound for the system output *y(k),* illustrating the progression of the system's output trajectory over time.

Taking into account inequalities (43) and (44), we can suggest the following state-space model (45):

$$\begin{cases} [A_1^c A_1^d] \begin{bmatrix} x_c(k) \\ x_d(k) \end{bmatrix}, , [A_2^c A_2^d] \begin{bmatrix} x_c(k-1) \\ x_d(k-1) \end{bmatrix} + [B_1^c B_1^d] \begin{bmatrix} v_c(k) \\ v_d(k) \end{bmatrix} + [T_x] \\ [C_1^c C_1^d] \begin{bmatrix} y_c(k) \\ y_d(k) \end{bmatrix}, , [C_2^c C_2^d] \begin{bmatrix} x_c(k) \\ x_d(k) \end{bmatrix} + [D_1^c D_1^d] \begin{bmatrix} v_c(k) \\ v_d(k) \end{bmatrix} + [T_y] \end{cases} \quad (45)$$

With:

$$A_1^c = \begin{pmatrix} -w_{vx}^{-cc} \\ -w_{vx}^{-dc} \\ -w_{xx}^{-cc} \\ -w_{xx}^{-dc} \\ -I \end{pmatrix}, A_2^c = \begin{pmatrix} 0 \\ 0 \\ w_{xx}^{+cc} \\ w_{xx}^{+dc} \\ -I \end{pmatrix}, \; B_1^c = \begin{pmatrix} w_{vx}^{+cc} \\ w_{vx}^{+dc} \\ 0 \\ 0 \\ 0 \end{pmatrix} \quad (46)$$

$$A_1^d = \begin{pmatrix} -w_{vx}^{-cd} \\ -w_{vx}^{-dd} \\ -w_{xx}^{-cd} \\ -w_{xx}^{-dd} \\ -I \end{pmatrix}, A_2^d = \begin{pmatrix} 0 \\ 0 \\ w_{xx}^{+cd} \\ w_{xx}^{+dd} \\ -I \end{pmatrix}, T_x = \begin{pmatrix} -T_{vx} \\ -T_{vx} \\ -T_{xx} \\ -T_{xx} \\ 0 \end{pmatrix}, \quad B_2^d = \begin{pmatrix} w_{vx}^{+cd} \\ w_{vx}^{+dd} \\ 0 \\ 0 \\ 0 \end{pmatrix} \quad (47)$$

$$C_1^c = \begin{pmatrix} -w_{xy}^{-cc} \\ -w_{xy}^{-dc} \\ -w_{vy}^{-cc} \\ -w_{vy}^{-dc} \\ -I \end{pmatrix}, C_2^c = \begin{pmatrix} w_{xy}^{+cc} \\ w_{xy}^{+dc} \\ 0 \\ 0 \\ -I \end{pmatrix}, T_y = \begin{pmatrix} -T_{xy} \\ -T_{xy} \\ -T_{vy} \\ -T_{vy} \\ 0 \end{pmatrix}, \quad D_1^c = \begin{pmatrix} 0 \\ 0 \\ w_{vx}^{+cc} \\ w_{vx}^{+dc} \\ -I \end{pmatrix} \quad (48)$$

$$C_1^d = \begin{pmatrix} -w_{xy}^{-cd} \\ -w_{xy}^{-dd} \\ -w_{vy}^{-cd} \\ -w_{vy}^{-dd} \\ -I \end{pmatrix}, C_2^d = \begin{pmatrix} w_{xy}^{+cd} \\ w_{xy}^{+dd} \\ 0 \\ 0 \\ -I \end{pmatrix}, D_1^d = \begin{pmatrix} 0 \\ 0 \\ w_{vx}^{+cd} \\ w_{vx}^{+dd} \\ 0 \end{pmatrix} \quad (49)$$

Analysis of the system's trajectory and dynamic behavior can be carried out by simulating the state model (45). The suggested approach (48) offers the possibility of defining initiation dates $x_c(k$,$x_d(k)$, $y_c(k)$ and $y_d(k)$ from previous dates $x_c(k-1)$, $x_d(k-1)$,$y_c(k-1)$ and $y_d(k-1)$ as well as system inputs $v_c(k)$ and $v_d(k)$. These trigger dates define the system state.

Where:

- *x(k):* Estimation of the state vector at time k
- *v(k):* (Estimated) input vector for time k
- *A, B:* Matrices of dating models reflecting system restrictions.

The inequality takes into account cumulative time constraints.

5. input and state-estimator design

5.1. Objective

In the context of hybrid systems, involving both continuous and discrete dynamics, accurate estimation of the internal state and unknown inputs is crucial for monitoring, control and fault diagnosis. In many practical applications, it is often impossible to directly measure all state variables or external inputs due to physical, technological or cost constraints. Consequently, the development of an estimator capable of reconstructing these variables from the available measurements becomes essential.

In the system considered in this study, the state and input estimation problem is addressed using a representation based on matrix inequalities. These inequalities provide a framework for modeling the hybrid behavior of the system while integrating possible disturbances or failures. To solve this problem, we propose the counter approach and dater approach, which offers a way of tracking the evolution of the system's state and estimating unknown inputs.

This section aims to synthesize a new form of observer used to estimate the state of the system and its inputs. This observer is composed of two matrix inequalities:
The first is used to evaluate the state of the system, while the second is used to reconstruct its inputs. The observer proposed here is similar to the state observer used for continuous systems, and has been developed in this article using counter- and date-based methods.
Throughout this work, the estimated parameters are described by the symbol 'Λ'.

5.2. Counter approach

In this framework, counter evolution is governed by a set of matrix inequalities encoding the logical and temporal relationships between system events. By analyzing the variation of these counters from the available measurements, we can reconstruct the trajectories of hidden state variables and estimate unknown inputs.

One of the main advantages of the counter-based approach is its ability to handle systems with a high degree of switching or mode transitions, characteristic of hybrid systems. This approach is also particularly effective in systems where continuous measurements are rare, and where the timing and order of events provide significant information on system behavior.

The state observer synthesis approach is based on transforming the inequalities used to simulate the system into suitable formats. Indeed, to reconstitute the state and inputs of the system, we calculate them from the known output. Details of the estimator's design are given below.

$$\begin{matrix} \hat{x_c}(t) \le \hat{x_c}(t+1) \\ \hat{x_d}(t) \le \hat{x_d}(t+1) \end{matrix} \quad (50)$$

$$\begin{matrix} \hat{v_c}(t) \le \hat{y_c}(t) \\ \hat{v_d}(t) \le \hat{y_d}(t) \end{matrix} \quad (51)$$

Inequalities (8) to (15), (50) and (51) can be gathered to obtain inequalities (52) and (53).

$$\begin{pmatrix} w_{vy}^{+cc} & w_{vy}^{+cd} \\ w_{vy}^{+dc} & w_{vy}^{+dd} \\ w_{vx}^{+cc} & w_{vx}^{+cd} \\ w_{vx}^{+dc} & w_{vx}^{+dd} \\ I & I \end{pmatrix} \begin{pmatrix} \hat{v_c}(t) \\ \hat{v_d}(t) \end{pmatrix} \le \begin{pmatrix} m_{vy} \\ m_{vy} \\ m_{vx} \\ m_{vx} \\ 0 \end{pmatrix} - \begin{pmatrix} w_{vy}^{-cc} & w_{vy}^{-cd} & 0 & 0 \\ w_{vy}^{-dc} & w_{vy}^{-dd} & 0 & 0 \\ 0 & 0 & w_{vx}^{-cc} & w_{vx}^{-cd} \\ 0 & 0 & w_{vx}^{-dc} & w_{vx}^{-dd} \\ I & I & 0 & 0 \end{pmatrix} \begin{pmatrix} \hat{y_c}(t) \\ \hat{y_d}(t) \\ \hat{x_c}(t) \\ \hat{x_d}(t) \end{pmatrix} \quad (52)$$

$$\begin{pmatrix} w_{xy}^{+cc} & w_{xy}^{+cd} \\ w_{xy}^{+dc} & w_{xy}^{+dd} \\ w_{xx}^{+cc} & w_{xx}^{+cd} \\ w_{xx}^{+dc} & w_{xx}^{+dd} \\ I & I \end{pmatrix} \begin{pmatrix} \hat{x_c}(t) \\ \hat{x_d}(t) \end{pmatrix} \le \begin{pmatrix} m_{xy} \\ m_{xy} \\ m_{xx} \\ m_{xx} \\ 0 \end{pmatrix} - \begin{pmatrix} w_{xy}^{-cc} & w_{xy}^{-cd} & 0 & 0 \\ w_{xy}^{-dc} & w_{xy}^{-dd} & 0 & 0 \\ 0 & 0 & w_{xx}^{-cc} & w_{xx}^{-cd} \\ 0 & 0 & w_{xx}^{-dc} & w_{xx}^{-dd} \\ 0 & 0 & I & I \end{pmatrix} \begin{pmatrix} \hat{y_c}(t) \\ \hat{y_d}(t) \\ \hat{x_c}(t+1) \\ \hat{x_d}(t+1) \end{pmatrix} \quad (53)$$

Inequality (52) proposes a lower bound for the system input *v(t),* while inequality (53) also offers a lower bound for the state vector *x(t).*

Based on these disparities, the following can be suggested as a state observer:

$$\begin{cases} [A_{01}^c\, A_{01}^d] \begin{bmatrix} \hat{x_c}(t) \\ \hat{x_d}(t) \end{bmatrix}, , [A_{02}^c\, A_{02}^d] \begin{bmatrix} \hat{x_c}(t+1) \\ \hat{x_d}(t+1) \end{bmatrix} + [C_{01}^c\, C_{01}^d] \begin{bmatrix} \hat{y_c}(t) \\ \hat{y_d}(t) \end{bmatrix} + [M_{0x}] \\ [B_{01}^c\, B_{01}^d] \begin{bmatrix} \hat{v_c}(t) \\ \hat{v_d}(t) \end{bmatrix}, , [B_{02}^c\, B_{02}^d] \begin{bmatrix} \hat{x_c}(t) \\ \hat{x_d}(t) \end{bmatrix} + [D_{01}^c\, D_{01}^d] \begin{bmatrix} \hat{y_c}(t) \\ \hat{y_d}(t) \end{bmatrix} + [M_{0y}] \end{cases} \quad (54)$$

Where:

$$A_{01}^c = \begin{pmatrix} w_{xy}^{+cc} \\ w_{xy}^{+dc} \\ w_{xx}^{+cc} \\ w_{xx}^{+dc} \\ I \end{pmatrix}, A_{02}^c = \begin{pmatrix} 0 \\ 0 \\ w_{xx}^{-cc} \\ w_{xx}^{-dc} \\ I \end{pmatrix}, M_{0x} = \begin{pmatrix} m_{xx} \\ m_{xx} \\ m_{xy} \\ m_{xy} \\ 0 \end{pmatrix}, \quad (55)$$

$$C_{01}^c = \begin{pmatrix} w_{xy}^{-cc} \\ w_{xy}^{-dc} \\ 0 \\ 0 \\ 0 \end{pmatrix}$$

$$A_{01}^d = \begin{pmatrix} w_{xy}^{-cd} \\ w_{xy}^{-dd} \\ w_{xx}^{-cd} \\ w_{xx}^{-dd} \\ I \end{pmatrix}, A_{02}^d = \begin{pmatrix} 0 \\ 0 \\ w_{xx}^{-cd} \\ w_{xx}^{-dd} \\ 0 \end{pmatrix}, \; C_{01}^d = \begin{pmatrix} w_{xy}^{-cd} \\ w_{xy}^{-dd} \\ 0 \\ 0 \\ 0 \end{pmatrix} \quad (56)$$

$$B_{01}^c = \begin{pmatrix} w_{vy}^{+cc} \\ w_{vy}^{+dc} \\ w_{vx}^{+cc} \\ w_{vx}^{+dc} \\ I \end{pmatrix}, D_{01}^c = \begin{pmatrix} w_{vy}^{-cc} \\ w_{vy}^{-dc} \\ 0 \\ 0 \\ 0 \end{pmatrix}, M_{0u} = \begin{pmatrix} m_{vy} \\ m_{vy} \\ m_{vx} \\ m_{vx} \\ 0 \end{pmatrix}, \quad (57)$$

$$B_{02}^c = \begin{pmatrix} 0 \\ 0 \\ w_{vx}^{-cc} \\ w_{vx}^{-dc} \\ 0 \end{pmatrix}$$

$$B_{01}^d = \begin{pmatrix} w_{vy}^{+cd} \\ w_{vy}^{+dd} \\ w_{vx}^{+cd} \\ w_{vx}^{+dd} \\ I \end{pmatrix}, D_{01}^d = \begin{pmatrix} w_{vy}^{-cd} \\ w_{vy}^{-dd} \\ 0 \\ 0 \\ 0 \end{pmatrix}, \; B_{02}^d = \begin{pmatrix} 0 \\ 0 \\ w_{vx}^{-cd} \\ w_{vx}^{-dd} \\ 0 \end{pmatrix} \quad (58)$$

The suggested observation system evaluates the values *of* $x_c(t)$, $x_d(t)$, $v_c(t)$, $v_d(t)$ from their posterior times $x_c(t+1)$, $x_d(t+1)$, $y_c(t+1)$, $y_d(t+1)$ and its output at time $y_c(t)$, $y_d(t)$.

5.2. Dater approach

For the synthesis of the state observer based on the so-called dater approach, it is essential to carefully modify the inequalities specified in equations (31) to (38). The aim is to facilitate simultaneous evaluation of the hybrid system's internal state and unmeasured inputs, based solely on the observations collected at the output. This is a vital phase for system diagnosis, management and control, especially when faced with complex dynamic constraints or operational uncertainties.

The state estimator is designed on the basis of a temporal formalism subject to inequalities, which highlight the lower and upper bounds of the transition times. These constraints are derived from the simulated model and reflect the observed temporal behavior of the system. Evaluation is then carried out by comparing these limits with the temporal information available during observation, with the aim of limiting the totality of temporal paths allowed by the system, and deducing a range of uncertainty concerning internal states and triggered events. This method is particularly suitable for systems where events cannot be observed directly, but whose impacts on outputs can be linked to internal transitions via defined temporal relations

We begin by setting out the conditions for non-decline as follows:

$$\begin{aligned} \hat{x}_c(k) &\le \hat{x}_c(k+1) \\ \hat{x}_d(k) &\le \hat{x}_d(k+1) \end{aligned} \tag{59}$$

$$\begin{aligned} \hat{v}_c(k) &\le \hat{y}_c(k) \\ \hat{v}_d(k) &\le \hat{y}_d(k) \end{aligned} \tag{60}$$

Inequalities (31) to (38), (59) and (60) are gathered to obtain inequalities (61) and (62).

$$\begin{pmatrix} w_{vy}^{+cc} & w_{vy}^{+cd} \\ w_{vy}^{+dc} & w_{vy}^{+dd} \\ w_{vx}^{+cc} & w_{vx}^{+cd} \\ w_{vx}^{+dc} & w_{vx}^{+dd} \end{pmatrix} \begin{pmatrix} \hat{v}_c(k) \\ \hat{v}_d(k) \end{pmatrix} \le \begin{pmatrix} w_{vy}^{-cc} & w_{vy}^{-cd} & 0 & 0 \\ w_{vy}^{-dc} & w_{vy}^{-dd} & 0 & 0 \\ 0 & 0 & w_{vx}^{-cc} & w_{vx}^{-cd} \\ 0 & 0 & w_{vx}^{-dc} & w_{vx}^{-dd} \end{pmatrix} \begin{pmatrix} \hat{y}_c(k) \\ \hat{y}_d(k) \\ \hat{x}_c(k) \\ \hat{x}_d(k) \end{pmatrix} - \begin{pmatrix} T_{vy} \\ T_{vy} \\ T_{vx} \\ T_{vx} \end{pmatrix} \tag{61}$$

$$\begin{pmatrix} w_{xy}^{+cc} & w_{xy}^{+cd} \\ w_{xy}^{+dc} & w_{xy}^{+dd} \\ w_{xx}^{-cc} & w_{xx}^{-cd} \\ w_{xx}^{-dc} & w_{xx}^{-dd} \end{pmatrix} \begin{pmatrix} \hat{x}_c(k) \\ \hat{x}_d(k) \end{pmatrix} \le \begin{pmatrix} w_{xy}^{-cc} & w_{xy}^{-cd} & 0 & 0 \\ w_{xy}^{-dc} & w_{xy}^{-dd} & 0 & 0 \\ 0 & 0 & w_{xx}^{+cc} & w_{xx}^{+cd} \\ 0 & 0 & w_{xx}^{+dc} & w_{xx}^{+dd} \end{pmatrix} \begin{pmatrix} \hat{y}_c(k) \\ \hat{y}_d(k) \\ \hat{x}_c(k+1) \\ \hat{x}_d(k+1) \end{pmatrix} - \begin{pmatrix} T_{xy} \\ T_{xy} \\ T_{xx} \\ T_{xx} \end{pmatrix} \tag{62}$$

Inequality (61) allows estimation of the system input by determining a lower bound for *v(k).* Inequality (62) estimates the state by calculating a lower bound for *x(k).*

Based on inequalities (61) and (62), we can suggest the following state observer:

$$\begin{cases} [A_{01}^c\, A_{01}^d] \begin{bmatrix} \hat{x}_c(k) \\ \hat{x}_d(k) \end{bmatrix}, , [A_{02}^c\, A_{02}^d] \begin{bmatrix} \hat{x}_c(k+1) \\ \hat{x}_d(k+1) \end{bmatrix} + [C_{01}^c\, C_{01}^d] \begin{bmatrix} \hat{y}_c(k) \\ \hat{y}_d(k) \end{bmatrix} + [T_{0x}] \\ [B_{01}^c\, B_{01}^d] \begin{bmatrix} \hat{v}_c(k) \\ \hat{v}_d(k) \end{bmatrix}, , [B_{02}^c\, B_{02}^d] \begin{bmatrix} \hat{x}_c(k) \\ \hat{x}_d(k) \end{bmatrix} + [D_{01}^c\, D_{01}^d] \begin{bmatrix} \hat{y}_c(k) \\ \hat{y}_d(k) \end{bmatrix} + [T_{0v}] \end{cases} \tag{63}$$

Where:

$$A_{01}^c = \begin{pmatrix} w_{xy}^{+cc} \\ w_{xy}^{+dc} \\ w_{xx}^{+cc} \\ w_{xx}^{+dc} \\ I \end{pmatrix}, A_{02}^c = \begin{pmatrix} 0 \\ 0 \\ w_{xx}^{-cc} \\ w_{xx}^{-dc} \\ I \end{pmatrix}, T_{0x} = \begin{pmatrix} -T_{xx} \\ -T_{xx} \\ -T_{xy} \\ -T_{xy} \\ 0 \end{pmatrix}, \tag{64}$$

$$C_{01}^c = \begin{pmatrix} w_{xy}^{-cc} \\ w_{xy}^{-dc} \\ 0 \\ 0 \\ 0 \end{pmatrix}$$

$$A_{01}^d = \begin{pmatrix} w_{xy}^{+cd} \\ w_{xy}^{+dd} \\ w_{xx}^{cd} \\ w_{xx}^{dd} \\ I \end{pmatrix}, A_{02}^d = \begin{pmatrix} 0 \\ 0 \\ w_{xx}^{+cd} \\ w_{xx}^{+dd} \\ I \end{pmatrix}, C_{01}^d = \begin{pmatrix} w_{xy}^{-cd} \\ w_{xy}^{-dd} \\ 0 \\ 0 \\ 0 \end{pmatrix} \tag{65}$$

$$B_{01}^c = \begin{pmatrix} w_{vy}^{+cc} \\ w_{vy}^{+dc} \\ w_{vx}^{+cc} \\ w_{vx}^{+dc} \\ I \end{pmatrix}, B_{02}^c = \begin{pmatrix} 0 \\ 0 \\ w_{vx}^{-cc} \\ w_{vx}^{-dc} \\ I \end{pmatrix}, T_{0v} = \begin{pmatrix} -T_{vx} \\ -T_{vx} \\ -T_{vy} \\ -T_{vy} \\ 0 \end{pmatrix} \tag{66}$$

$$D_{01}^c = \begin{pmatrix} w_{vy}^{-cc} \\ w_{vy}^{-dc} \\ 0 \\ 0 \\ 0 \end{pmatrix}$$

$$B_{01}^d = \begin{pmatrix} w_{vy}^{+cd} \\ w_{vy}^{+dd} \\ w_{vx}^{+cd} \\ w_{vx}^{+dd} \\ I \end{pmatrix}, B_{02}^d = \begin{pmatrix} 0 \\ 0 \\ w_{vx}^{-cd} \\ w_{vx}^{-dd} \\ I \end{pmatrix}, D_{02}^d = \begin{pmatrix} w_{vy}^{-cd} \\ w_{vy}^{-dd} \\ 0 \\ 0 \\ 0 \end{pmatrix} \tag{67}$$

The algebraic model for evaluating system input and state is described by the state observer (66). It offers the possibility of evaluating dates $x_c(k)$, $x_d(k)$ and $v_c(k)$, $v_d(k)$ based on later dates $x_c(k+1)$, $x_d(k+1)$ and $v_c(k+1)$, $v_d(k+1)$ while assuming that the system response is known: $y_c(k)$, $y_d(k)$.

6. Application to a micro-Grid with four distributed generators (4-DGS)

This section presents the application of HPN modeling and the proposed observer design to a microgrid system integrating four distributed energy sources (4-DG). As shown in Figure 1, the microgrid integrates a wind turbine, a battery storage system, a photovoltaic solar panel and a diesel generator. These energy sources are coordinated to ensure a stable and reliable power supply, even in the presence of environmental fluctuations or variations in energy demand [12].

In order to examine the robustness and efficiency of the proposed hybrid Petri net model (model 22) and the associated observer (model 31), we adopt a residual-based validation approach. In this situation, residuals refer to the difference between the estimated values provided by the observer and the actual values obtained by simulating the model. When these residuals are zero or negligible, this means that the model and observer produce consistent results, validating the accuracy of the structural model and estimation algorithm.

In this specific case study, we focus solely on the counter-based method for building observers, as it is particularly suited to tracking discrete transitions and energy flows in the microgrid. The estimation process therefore relies on reformulated inequalities derived from the simulation model to reconstruct the system state and inputs from output measurements alone.

Each location and transition in the HPN model (Figure 1) is associated with precise physical meanings corresponding to the components and operating modes of the microgrid. Table 1 provides a detailed description of these elements, indicating for each energy source the associated locations, transitions and operational conditions. This mapping provides a clear understanding of the energy flows modeled, and facilitates the implementation of fault detection or energy optimization strategies. For a full explanation of the model structure and its components, please refer to [12].

The microgrid examined here represents a typical example of an intelligent energy system based on diverse, complementary sources. The wind turbine generates electricity in proportion to wind speed, based on operating modes defined by critical thresholds of minimum, nominal and maximum wind speeds. The solar panel converts the sun's energy into electricity, with output varying according to irradiance, as soon as the latter exceeds a minimum level. Despite its high economic and ecological cost, the diesel generator is used when renewable energy production fails to meet demand, guaranteeing uninterrupted service. These elements interact dynamically under the management of an integrated control system, which considers not only the physical and operational constraints of each source, but also the overall goals of efficiency, reliability and sustainability of the energy system. HPN modeling, which takes into account both continuous (energy flow) and discrete (condition or mode changes) aspects, is capable of capturing this hybrid complexity. It offers a valuable tool for the simulation, study and management of intelligent energy systems.

- V: current wind speed (in m/s), input variable.
- V_a: minimum wind speed for the turbine to start up (start-up speed).
- V_n: wind speed at which the turbine reaches maximum power (nominal speed).
- $f_{(V)}$: increasing function of wind speed, giving the energy produced in normal mode.
- v_{11}: energy production rate of the turbine in normal mode.
- v_{12}: energy production rate in maximum power mode, equal to E_{max}.
- E_{max}: maximum power the wind turbine can produce.
- E_w: energy produced by the wind turbine.
- E_{solar}: energy produced by solar panel.
- v_{13}: energy production rate of solar panel.
- v_{15}: battery discharge rate.
- v_{16}: energy production rate of diesel generator when running.
- v_{wp}: instantaneous combined production of wind turbine and solar panel ($v_{11} + v_{13}$ or $v_{12} + v_{13}$).
- v_{17}: system energy demand.
- $M_{(p8)}$: amount of energy available.
- $M_{(p11)}$: energy deficit.

Table 1 HPN Model: Subsystems, Places, Transitions, and Operating Modes.

Energy Source	Places (p_i)	Transitions (t_i)	Operating Modes
Wind Turbine	p_1, p_2, p_3	$t_1 - t_6, t_{11} - t_{12}$	Normal Mode ($V_a<V<V_n$) → Transition t_{11} activated with ($v_{11} = f(V)$) Maximum Power Mode ($V>V_n$) → Transition t_{12} activated with ($v_{12} = E_{max}$) Shutdown Mode ($V<a$) → No transition occurs, the output energy ($E_w = 0$)
Photo- voltaic Cell	p_4, p_5	t_7, t_8, t_{13}	Active Mode (ON) → t_{13} activated at a rate v_{13} that is affected by solar irradiation. Inactive Mode (OFF) → $E_{solar} = 0$
Battery	p_9, p_{10}	t_{14}, t_{15}	Charging (t_{14}) → The rate of transition fires is v_{14} Storage → No transition is started. Discharging (t_{15}) → The rate of transition fires is v_{15}
Diesel Generator	p_6, p_7	t_9, t_{10}, t_{16}	Energy Production → p_6 holds a token, t_{16} activated with v_{16} Shutdown → No firing
Load Management	p_8, p_{11}	t_{17}, t_{18}	Sufficient Energy ($M(p_8)>0$) → The system operates under normal conditions. ($M(p_{11}) > 0$) → both the diesel generator and battery are activated. Excess Energy ($v_{wp}>v_{17}$) → The battery switches to charging mode and the generator stops.

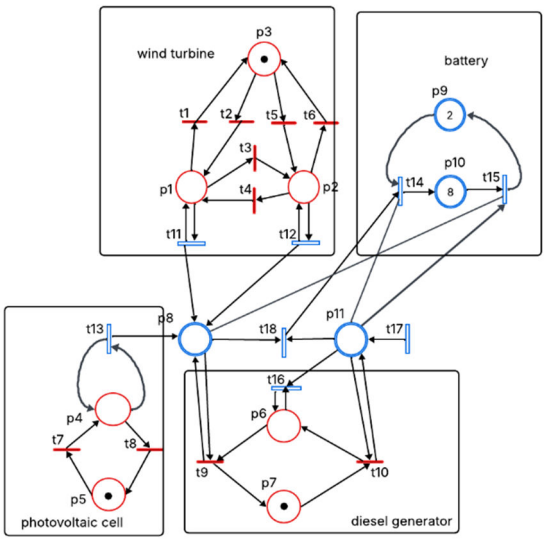

Fig. 1 PN-based model for a microgrid with four distributed generators (4-DGs).

The inclusion of four distributed generators (4-DG) in a microgrid represents a contemporary and adaptable structure that meets the growing demand for energy independence, operational flexibility and ecological sustainability. This type of hybrid device is particularly suited to isolated or critical contexts, such as rural areas not connected to the main grid, hospital facilities or military camps, where constancy of energy supply is paramount. The use of hybrid Petri nets for modeling not only enables accurate representation of the mixed dynamics (discrete and continuous) associated with energy flows and operational modes, but also the simulation of degraded operation, optimization or transition scenarios between different sources. Indeed, one of the main challenges lies in optimal coordination between generators to avoid energy losses, minimize reliance on fossil sources, and ensure rapid response to variations in demand. What's more, the state transitions modeled in HPN make it possible to include switching times, recharging or start-up constraints, as well as operating priorities according to defined energy policies. This approach also facilitates the integration of intelligent or predictive management algorithms, which can be used for automated decision-making in embedded energy management systems.

Finally, the designed observer enables the internal state of the system to be monitored based solely on measured outputs, which is essential for remote monitoring, predictive maintenance, or early detection of potential failures.

Inequalities (68) model the system behavior:

$$T_1(k) + T_3(k) + T_{11}(k) \leq T_{11}(k-1) + T_4(k-1) + T_2(k-1) + 1 \quad (68a)$$

$$T_4(k) + T_6(k) + T_{12}(k) \leq T_3(k-1) + T_8(k-1) + T_{12}(k-1) + 1 \quad (68b)$$

$$T_5(k) + T_2(k) \leq T_6(k-1) + T_1(k-1) + 1 \quad (68c)$$

$$T_{18}(k) + T_{14}(k) + T_9(k) \leq T_{13}(k-1) + T_{11}(k-1) + T_{12}(k-1) + T_9(k-1) + 1 \quad (68d)$$

$$T_{10}(k) + T_{16}(k) + T_{18}(k) + T_{15}(k) \leq T_{17}(k-1) + T_{10}(k-1) + 1 \quad (68e)$$

$$T_{16}(k) + T_9(k) \leq T_{10}(k-1) + T_{16}(k-1) + 1 \quad (68f)$$

$$T_{10}(k) \leq T_9(k-1) + 1 \quad (68g)$$

$$T_{15}(k) \leq T_{14}(k-1) + 8 \quad (68h)$$

$$T_{14}(k) \leq T_{15}(k-1) + 2 \quad (68i)$$

$$T_7(k) \leq T_8(k-1) + 1 \quad (68j)$$

$$T_{13}(k) + T_8(k) \leq T_7(k-1) + T_{13}(k-1) + 1 \quad (68k)$$

For this HPN model, we can rewrite inequalities (68) using the equivalent structure of inequalities (69):

$$A_1 T(k) \leq A_2 T(k-1) + M \quad (69)$$

Where:

$$A_1 = \begin{pmatrix} 1&0&1&0&0&0&0&0&0&0&1&0&0&0&0&0&0&0 \\ 0&0&0&1&0&1&0&0&0&0&0&1&0&0&0&0&0&0 \\ 1&1&0&0&1&0&0&0&0&0&0&0&0&0&0&0&0&0 \\ 0&0&0&0&0&0&0&0&1&0&1&1&0&1&0&0&0&1 \\ 0&0&0&0&0&0&0&0&0&1&1&0&0&0&1&1&0&0 \\ 0&0&0&0&0&0&0&0&1&1&0&0&0&0&0&1&0&0 \\ 0&0&0&0&0&0&0&0&1&0&0&0&0&0&0&0&0&0 \\ 0&0&0&0&0&0&0&0&0&0&0&0&0&0&1&0&0&0 \\ 0&0&0&0&0&0&0&0&0&0&0&0&0&0&1&0&0&0 \\ 0&0&0&0&0&0&1&0&0&0&0&0&0&0&0&0&0&0 \\ 0&0&0&0&0&0&0&1&1&0&0&0&1&0&0&0&0&0 \end{pmatrix}$$

$$A_2 = \begin{pmatrix} 0&1&0&1&0&0&0&0&0&0&1&0&0&0&0&0&0&0 \\ 0&0&1&0&0&0&0&1&0&0&0&1&0&0&0&0&0&0 \\ 1&0&0&0&0&1&0&0&0&0&0&0&0&0&0&0&0&0 \\ 0&0&0&0&0&0&0&0&1&0&1&1&1&0&0&0&0&0 \\ 0&0&0&0&0&0&0&0&0&1&1&0&0&0&0&0&0&0 \\ 0&0&0&0&0&0&0&0&1&0&0&0&0&0&0&1&0&0 \\ 0&0&0&0&0&0&0&0&1&0&0&0&0&0&0&0&0&0 \\ 0&0&0&0&0&0&0&0&0&0&0&0&0&0&1&0&0&0 \\ 0&0&0&0&0&0&0&0&0&0&0&0&0&0&1&0&0&0 \\ 0&0&0&0&0&0&0&1&0&0&0&0&0&0&0&0&0&0 \\ 0&0&0&0&0&0&1&0&0&0&0&0&1&0&0&0&0&0 \end{pmatrix}$$

$$M = (1\ 1\ 1\ 1\ 1\ 1\ 1\ 8\ 2\ 1\ 1)^T$$

And

$$T = (T_1\ T_2\ T_3\ T_4\ T_5\ T_6\ T_7\ T_8\ T_9\ T_{10}\ T_{11}\ T_{12}\ T_{13}\ T_{14}\ T_{15}\ T_{16}\ T_{17}\ T_{18})^T$$

Input transitions represent exogenous events or energy flows that directly influence the evolution of the system without being triggered by internal conditions. These transitions are considered to be known during the simulation, as they reflect controllable or observable actions (such as energy demand, energy injection by a renewable source, or the triggering of a generator).

The choice of input transitions was based on several essential criteria:

- Direct access to measurement: the chosen transitions correspond to data available in real time from sensors or management systems.
- Significant impact on system dynamics: they strongly influence the state of the network (e.g. rapid change in power injected or withdrawn).
- Representation of sources of uncertainty: some incoming transitions allows to model the effect of intermittent sources (such as solar or wind power), which is necessary to assess the robustness of the estimation.

6.1. State simulation

In this studied case, transitions T_1, T_7, T_9, T_{14} and T_{17} were selected as input transitions, as they correspond respectively to energy actions from active or regulating sources (photovoltaic, battery, consumption, DC load flow). This choice makes it possible to control the system simulation while ensuring that the temporal evolution remains consistent with the physical operation of the microgrid.

Table 2 summarizes the key parameters and starting values used in the simulation. These parameters are selected to represent the actual operating conditions of a 4-DG microgrid and constitute the input data for the state-space model presented in Section 4. Based on these values, the system is simulated as a function of 8 distinct time intervals *(k = 0 to 7).*

Parameter	Description	Initial Value	Max Value	Unit
T_1	Wind turbine trigger count	2	7	events
v_{11}	Wind energy production rate (approximate)	~0.5	1.0	kW
T_7	Solar production transitions	3	8	events
v_{13}	PV power production rate	0.75	1.2	kW
T_9	Diesel generator production trigger	4	9	events
v_{16}	Diesel generator production rate	2.5	6.3	kW
T_{14}	Battery charge transitions	5.0	10.5	events
v_{14}	Battery charge rate	~0.8	~1.5	kW
T_{15}	Battery discharge transitions	13.0	20.5	events
v_{15}	Battery discharge rate	~1.5	~2.2	kW
T_{17}	Load demand transitions	4.5	7.5	events
v_{17}	Energy demand	~1.0	~1.6	kW

Using the transitions T_1, T_7, T_9, T_{14} and T_{17} known for $(k) \in [0, ..., 7]$ and the initial state vector at $k = 0$, we can simulate the temporal progression of the system. Since transitions T_{14} and T_{17} are continuous, they are assigned real values to illustrate their influence on the system's evolution.

Table 3: Simulation of system trajectory over time.

T	0	1	2	3	4	5	6	7
T_1	2	3	3	4	5	5	6	7
T_2	2	3	4	4	5	6	6	7
T_3	3	3	4	4	5	6	6	7
T_4	3	4	4	5	5	6	6	7
T_5	4	4	5	5	6	7	7	8
T_6	6	7	8	9	10	11	12	13
T_7	3	3	4	5	6	6	7	8
T_8	7	8	9	9	10	11	12	13
T_9	4	4	6	6	7	7	8	9
T_{10}	5	6	7	7	8	8	9	10.0
T_{11}	2.0	2.3	2.8	3.1	3.5	4.0	4.5	5.0
T_{12}	6.0	6.2	6.6	7.0	7.5	8.0	8.6	9.0
T_{13}	4.0	4.5	5.0	5.4	5.9	6.5	7.1	7.8
T_{14}	5.0	6.0	7.5	7.9	8.3	8.5	9.0	10.5
T_{15}	13.0	14.0	15.5	16.0	17.0	18.0	19.5	20.5
T_{16}	2.5	3.0	3.5	4.0	4.8	5.2	5.8	6.3
T_{17}	4.5	4.9	5.3	6.0	6.8	7.1	7.3	7.5
T_{18}	2.1	4.50	5.50	6.11	7.17	8.42	9.33	10.23

6.2. State estimation

The following inequalities describe the behavior of the state estimator, derived by inverting the simulation constraints:

If we know the output transitions T_6, T_8, T_{10}, T_{15}, T_{17} and T_{18} for $k \in [0, ..., 7]$, we can predict how the system will evolve over time. Table 3 shows the results.

The following inequalities describe the behavior of the state estimator, derived by inverting the simulation constraints:

$$T_{11}(k-1) + T_4(k-1) + T_2(k-1) \geq T_1(k) + T_3(k) + T_{11}(k) - 1 \quad (70a)$$

$$T_3(k-1) + T_8(k-1) + T_{12}(k-1) \geq T_4(k) + T_6(k) + T_{12}(k) - 1 \quad (70b)$$

$$T_6(k-1) + T_1(k-1) \geq T_5(k) + T_2(k) - 1 \quad (70c)$$

$$T_{13}(k-1) + T_{11}(k-1) + T_{12}(k-1) + T_9(k-1) \geq T_{18}(k) + T_{14}(k) + T_9(k) - 1 \quad (70d)$$

$$T_{17}(k-1) + T_{10}(k-1) \geq T_{10}(k) + T_{16}(k) + T_{18}(k) + T_{15}(k) - 1 \quad (70e)$$

$$T_{10}(k-1) + T_{16}(k-1) \geq T_{16}(k) + T_9(k) - 1 \quad (70f)$$

$$T_9(k-1) \geq T_{10}(k) - 1 \quad (70g)$$

$$T_{14}(k-1) \geq T_{15}(k) - 8 \quad (70h)$$

$$T_{15}(k-1) \geq T_{14}(k) - 2 \quad (70i)$$

$$T_8(k-1) \geq T_7(k) - 1 \quad (70j)$$

$$T_7(k-1) + T_{13}(k-1) \geq T_{13}(k) + T_8(k) - 1 \quad (70k)$$

From Tables 3 and 4, it is clear that the system path is non-decreasing. The following section compares simulated and estimated results.

6.3. Analysis and comparison

This section provides an in-depth study of the estimated values for the transitions from T_1 to T_{18} during the discrete time interval from $k=0$ to $k=7$. The study provides an overview of the main trends, typical behaviors and overall robustness of the suggested model in terms of the various dynamic elements of the system.

Table 4 State estimation.

T	0	1	2	3	4	5	6	7
T_1	2	3	3	4	5	5	6	7
T_2	2	3	4	4	5	6	6	7
T_3	3	3	4	4	5	6	6	7
T_4	3	4	4	5	5	6	6	7
T_5	4	4	5	5	6	7	7	8
T_6	6	7	8	9	10	11	12	13
T_7	3	3	4	5	6	6	7	8
T_8	7	8	9	9	10	11	12	13
T_9	4	4	6	6	7	7	8	9
T_{10}	5	6	7	7	8	8	9	10.0
T_{11}	2.0	2.3	2.8	3.1	3.5	4.0	4.5	5.0
T_{12}	6.0	6.2	6.6	7.0	7.5	8.0	8.6	9.0
T_{13}	4.0	4.5	5.0	5.4	5.9	6.5	7.1	7.8
T_{14}	5.0	6.0	7.5	7.9	8.3	8.5	9.0	10.5
T_{15}	13.0	14.0	15.5	16.0	17.0	18.0	19.5	20.5
T_{16}	2.5	3.0	3.5	4.0	4.8	5.2	5.8	6.3
T_{17}	4.5	4.9	5.3	6.0	6.8	7.1	7.3	7.5
T_{18}	2.1	4.50	5.50	6.11	7.17	8.42	9.33	10.23

Transitions T_1 to T_5, T_{10} to T_{13} and T_{16} show regularity and solid progression throughout the observed period. These transitions confirm the robustness and consistency of the model, signaling that the system is running smoothly during these stages. The state estimates for these transitions closely follow the expected dynamics, with no significant deviations observed in the results. This suggests that the model effectively captures steady-state behavior and can be relied upon under such conditions.

Transitions T_6, T_8, T_{14} and T_{15} show more dynamic or critical behaviors that require special attention. These transitions are marked by more significant variations in system state, which may indicate the onset of instability or high sensitivity to certain inputs. These behaviors need to be closely monitored to avoid potential saturation or overload of the system, which could lead to performance errors. In particular, transitions T_6 and T_8 show higher volatility, suggesting that these phases require improved control mechanisms to maintain system stability.

Transition T_{17} remains inactive throughout the observation period. This inactivity may suggest several possible problems, such as an unfulfilled condition or a configuration error in the system. It is important to investigate the underlying causes of this inactivity to ensure that all system states and transitions are correctly accounted for, and to prevent potential faults or behaviors not accounted for in the model.

The T_{18} transition has a gradual response, which is particularly useful for control or accumulation functions. The gradual evolution of this transition makes it well suited to processes requiring smooth adjustments over time. This feature is essential for tasks such as energy accumulation or gradual state changes, where abrupt transitions are undesirable. The evolution of T_{18} also illustrates the model's ability to handle more gradual and predictable changes in the system.

The temporal evolution of transitions from T_1 to T_{18} is shown in Figure 2, highlighting the high accuracy of the proposed state model and observer. In particular, the observer provides accurate estimates of the simulated state, with estimated and simulated values perfectly aligned across all transitions. This indicates that the state estimation process is highly reliable and that there is no discrepancy between the estimated state and the actual state of the system. The accuracy of the model and observer is crucial for practical applications requiring precise system monitoring and control.

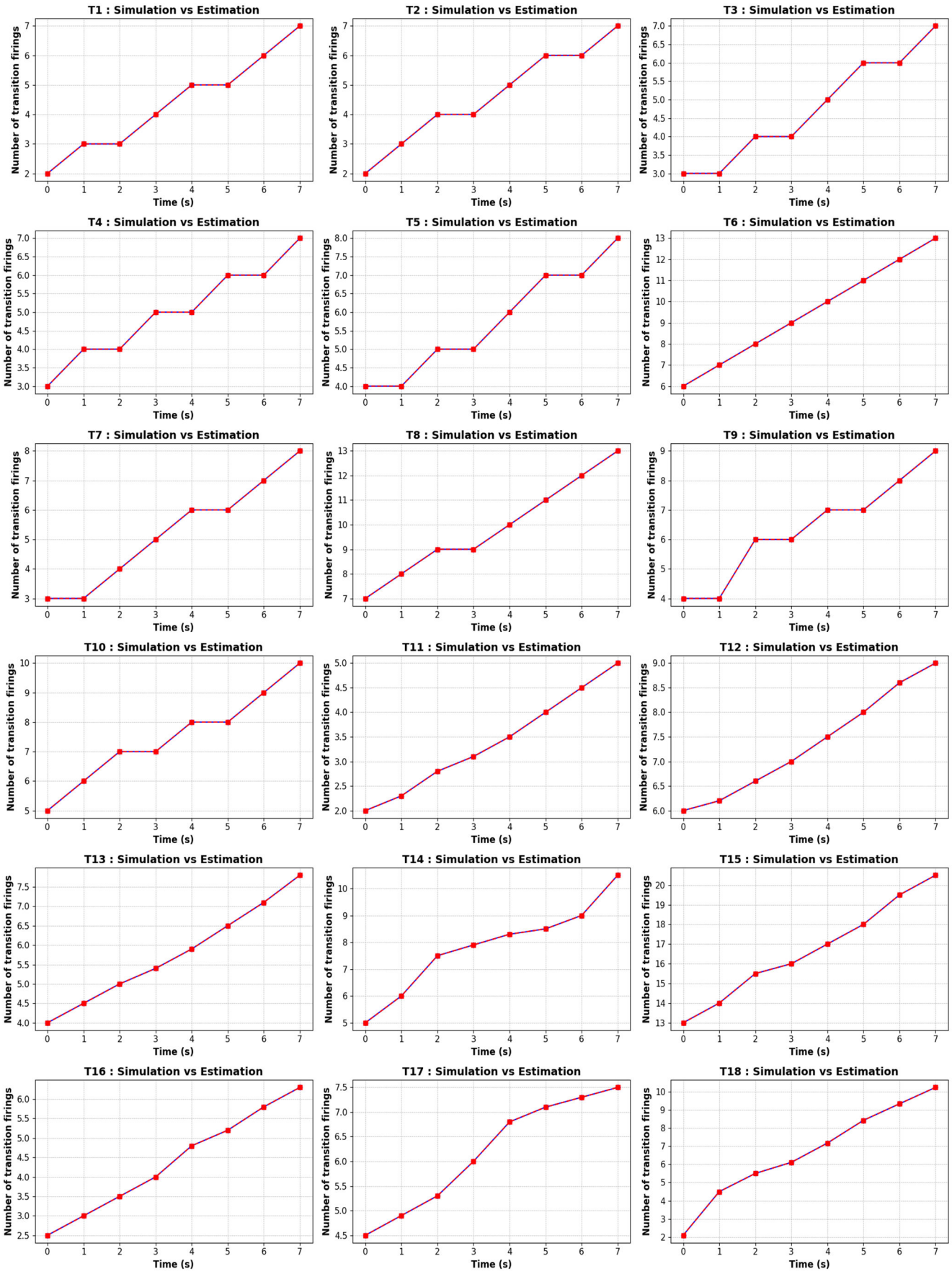

Fig 2. Evolution in time of simulated and estimated values of transitions T_1 to T_{18}.

Overall, the analysis confirms that the proposed state model, combined with the observer, is a comprehensive and reliable tool for estimating system dynamics. The consistent accuracy of estimates for all transitions suggests that the model is well suited to the monitoring and control of complex hybrid systems.

7. Conclusion

This research presents an innovative and methodical approach to modeling, investigating and controlling microgrids, based on the formalization of HPN. To illustrate precisely the hybrid dynamics of microgrids, which combine constant energy flows and discrete events, a mathematical model based on algebraic inequalities has been developed. This model offers a structured and adaptable representation of the interactions between the various dispersed energy sources and the system's operational restrictions.

At the same time, a state and input observer has been created to evaluate the internal state of the system and reconstruct inputs that have not been measured. This observer is essential for monitoring the system's behavior and detecting anomalies quickly, thereby helping to enhance the safety and reliability of the microgrid.

A case study involving a microgrid with four decentralized generators (4-DG): a wind turbine, a solar panel, a battery and a diesel generator confirmed the effectiveness of the suggested method. Simulation have shown that the observer succeeds in faithfully reconstructing system states in a variety of operational contexts, with virtually zero residual deviations in most situations. This validates the accuracy of the model and the estimation method employed.

There are a number of interesting avenues to explore in this study. In particular, the integration of machine learning techniques would enable adaptive, real-time state estimation, capable of dynamically adjusting to uncertainties, especially those linked to intermittent renewable energies. In addition, the optimization of microgrid control strategies, using predictive or intelligent algorithms, could significantly enhance the resilience, energy efficiency and fault tolerance of tomorrow's smart grids.

Thus, this work lays the foundations for a sound methodological framework combining formal modeling and intelligent supervision, and constitutes a promising tool for the design and management of next-generation energy systems.

Acknowledgements

The authors thank the anonymous reviewers for their valuable suggestions.

References

[1] Aydin, B. SWOT analysis of renewable energy. in *Proceedings of the 2014 International Conference and Utility Exhi- bition on Green Energy for Sustainable Development (ICUE 2014)*. (2014) 1-7.

[2] Cecati, C., Citro, C., Piccolo, A. and Siano, P., Smart operations of wind turbines and diesel generators according to economic criteria. *IEEE Transactions on Industrial Electronics*. 58 (2011) 4514–4525, doi: https://doi.org/10.1109/TIE.2011.2106100.

[3] Chamorro, H. R., Ordonez, C. A. and Jimenez, F. Coordinated control based Petri nets for microgrids including wind farms. in *Proceedings of the 2012 IEEE Power Electronics and Machines in Wind Applications (PEMWA)*. (2012) 1-6, doi: https://doi.org/10.1109/PEMWA.2012.6316370.

[4] Sava, A., Adjallah, K. H. and Lagaza, H., Hybrid Petri nets for modeling and control of multi-source energy conversion systems. in *2014 International Conference on Control, Decision, and Information Technology (CoDIT).* (2014), 516-521, doi: https://doi.org/10.1109/CoDIT.2014.6996947.

[5] Zhou, K., Yang, S., Chen, Z. and Ding, S., Optimal load distribution model of microgrid in the smart grid environment. *Renewable and Sustainable Energy Reviews*. 35 (2014) 304–310, doi: https://doi.org/10.1016/j.rser.2014.04.028.

[6] Paruchuri, V. K., Davari, A. and Feliachi, A. Hybrid modeling of power system using hybrid Petri nets. in *Proceedings of the 37th Southeastern Symposium on System Theory*. (2005) 221-224.

[7] Jr., A. G. P., Grid-Connected Self-Consumption Photovoltaic Solar Energy Production Design and Simulation Evaluation in Type II Climate Areas of Southeastern Philippines. *Journal of Renewable Energy and Smart Grid Technology*. 19 (2024) 31–39, doi: https://doi.org/10.69650/rast.2024.254448.

[8] Janthong, S. and Phukpattaranont, P., Recognition of Multiple Power Quality Disturbances Based on Discrete Wavelet Transform and Improved Long Short-Term Memory Networks. *Journal of Renewable Energy and Smart Grid Technology*. 19 (2024) 7–25, doi: https://doi.org/10.69650/rast.2024.255814.

[9] Susuk, S., Inchoorrun, N. ., Promjan, W. ., Chawananorasest, K. and Jamjumroon, S., Thermal Evaluation of Solar Dryer's Curve-Front Utilized Heat Transfer Analysis. *Journal of Renewable Energy and Smart Grid Technology*. 19 (2024) 45–56, doi: https://doi.org/10.69650/rast.2024.257468.

[10] Alla, H. and Ghomri, L. Modeling and simulation by hybrid Petri nets. in *Winter Simulation Conference (WSC '12).* (2012), 1-8.

[11] Allam, M. and Alla, H., From Hybrid Petri Nets to Automata. *Journal européen des systèmes automatisés*. 32 (1998) 1165–1185.

[12] David, R. and Alla, H., *Discrete, Continuous, and Hybrid Petri Nets*. Berlin, Germany: Springer-Verlag, 2005.

[13] Sharafi, S. M. and ELMekkawy, T., Multi-objective optimal design of hybrid renewable energy systems using pso-simulation based approach. *Renewable Energy*. 68 (2014) 67–79, doi: https://doi.org/10.1016/j.renene.2014.01.011.

[14] Hafez, O. and Bhattacharya, K., Optimal planning and design of a renewable energy based supply system for microgrids. *Renewable Energy*. 45 (2012) 7–15, doi: https://doi.org/10.1016/j.renene.2012.01.087.

[15] Huang, A. Q., Crow, M. L., Heydt, G. T., Zheng, J. P. and Dale, S. J., The future of renewable electric energy delivery and management (freedm) system: The Energy Internet. *Proceedings of the IEEE*. 99 (2011) 133–148.

[16] SURESH, A. K. and Giftson SAMUEL, G., Hybrid SFLA-ANN Method for Effective Power Management of Hybrid Power Sources in a Variety of Weather Scenarios. *Studies in Informatics and Control*. 33 (2024) 27-38, doi: https://doi.org/10.24846/v33i2y202403.

[17] Zarrad, O., Hajjaji, M. A. and Mansouri, M. N., Hardware Implementation of Hybrid Wind-Solar Energy System for Pumping Water Based on Artificial Neural Network Controller. *Studies in Informatics and Control.* 28 (2019) 35-44, doi: https://doi.org/10.24846/v28i1y201904.

[18] Soltani, K., Mlayeh, H. and Khedher, A. Modeling of Discrete Event Systems by Hybrid Petri Nets with Counter Approach. in *2023 IEEE International Conference on Artificial Intelligence and Green Energy (ICAIGE)*. (2023) 1-6, doi: https://doi.org/10.1109/ICAIGE58321.2023.10346525.

[19] Soltani, K., Khedher, A. and Khedher, A. Modeling and state estimation of discrete event systems using Hybrid Petri Nets. in *2023 20th International Multi-Conference on Systems,*

Signals & Devices (SSD). (2023) 1021-1026, doi: https://doi.org/10.1109/SSD58187.2023.10411246.

[20] Declerck, P., Counter approach for the estimation of optimal sequences in Partially Observable Untimed Petri Nets. *Discrete Event Dynamic Systems*. 31 (2021) 489–512, (2021). doi: https://doi.org/10.1007/s10626-021-00341-5.

[21] Affi, S., Guerfel, M. and Khedher, A. State Estimation of Discrete Events Systems Modeled by P-Timed FCF and BCF Petri Nets. in *2023 IEEE International Conference on Artificial Intelligence and Green Energy (ICAIGE).* 2023 (1-6), doi: https://doi.org/10.1109/ICAIGE58321.2023.10346272.

[22] Chaabene, M. and Fendri, D., Application of Hybrid Petri Nets for the Energy Dispatching of an Isolated Micro- Grid. *International Journal of Applied Metaheuristic Computing.* 11 (2020) 61-72, doi: https://doi.org/10.4018/IJAMC.2020010105.

[23] Halim, A., New Hybrid Petri Net application for modeling and analyzing complex smart microgrid system. *Journal of Engineering and Applied Sciences*. 13 (2018) 2713-2721.

[24] Xiaoyu, L., MengChu Z., Ahmed, C. A. and Jingchu, J., Hybrid Petri Nets for Modeling and Analysis of Microgrid Systems. *IEEE/CAA JOURNAL OF AUTOMATICA SINICA*. 3 (2016) 349-356.

[25] Hakiki, R. and Sekhri, L. Hybrid Petri nets based approach for analyzing complex dynamic systems. in *2010 International Conference on Machine and Web Intelligence*. (2010) 180-184.

[26] Glover, J. D., Sarma, M. S. and Overbye, T. (2011). *Power system analysis and design, SI version.* 5th edn., Cengage Learning, 2011.

[27] Chan, Y. -K. and Gu, J. -C. Modeling and simulation of microturbine and renewable energy resources for distributed generation system. in *2011 8th Asian Control Conference (ASCC).* (2011) 590-595.

[28] Khedher, A. and BenOthman, K., Modeling, simulation, estimation and boundedness analysis of discrete event systems. *Soft Computing*. 24 (2020) 4775-4789, doi: https://doi.org/10.1007/s00500-019-04231-9.

[29] Chouchane, A. and Declerck, P., Diagnosis on a sliding window for partially observable Petri nets. *Kybernetika*. 58 (2022) 479 -497, doi: https://doi.org/10.14736/kyb-2022-4-0479.

[30] Jr., A. G. P., Grid-Connected Self-Consumption Photovoltaic Solar Energy Production Design and Simulation Evaluation in Type II Climate Areas of Southeastern Philippines. *Journal of Renewable Energy and Smart Grid Technology*. 19 (2024) 1–11, doi: https://doi.org/10.69650/rast.2024.254448.

[31] Chouchane, A., Declerck, P., Khedher A. and Kamoun, A., Diagnosis Using an Estimation Method for Partially Observed Petri Net. *IFAC-PapersOnLine*. 50 (2017) 4348–4353, doi: https://doi.org/10.1016/j.ifacol.2017.08.855.

[32] Khedher, A. Estimation, diagnostic et commande tolérante aux défauts pour le systèmes non linéaires et à événements discrets. Habilitation thesis, Ecole Nationale d'Ingénieurs de Tunis (2021).

[33] David, R. and Alla, H., *Discrete, Continuous, and Hybrid Petri Nets.* 2nd edn., Springer-Verlag Berlin Heidelberg, 2010.

[34] David, R. Modeling of hybrid systems using continuous and hybrid Petri nets. in *the Seventh International Workshop on Petri Nets and Performance Models*. (1997) 24-33.